Structure, Vol. 8, 1025–1035, October, 2000, ©2000 Elsevier Science Ltd. All rights reserved. PII S0969-2126(00)00511-6

Crystal Structure of Hyaluronidase, a Major Allergen of Bee Venom

Zora Marković-Housley,*# Giuliana Miglierini,† Lyudmila Soldatova,‡ Pierre J. Rizkallah,§ Ulrich Müller,‖ and Tilman Schirmer*

*Division of Structural Biology
Biozentrum
University of Basel
CH-4056 Basel
Switzerland
†Polytech S.C.R.L.
34012 Trieste
Italy
‡Laboratory of Immunochemistry
US Food and Drug Administration
Rockville, Maryland 20852
§CCLRC Daresbury Laboratory
Daresbury, Warrington, Cheshire WA4 4AD
United Kingdom
‖Ziegler Hospital Bern
Medical Clinic
Postfach CH-3001 Bern
Switzerland

Summary

Background: Hyaluronic acid (HA) is the most abundant glycosaminoglycan of vertebrate extracellular spaces and is specifically degraded by a β-1,4 glycosidase. Bee venom hyaluronidase (Hya) shares 30% sequence identity with human hyaluronidases, which are involved in fertilization and the turnover of HA. On the basis of sequence similarity, mammalian enzymes and Hya are assigned to glycosidase family 56 for which no structure has been reported yet.

Results: The crystal structure of recombinant (Baculovirus) Hya was determined at 1.6 Å resolution. The overall topology resembles a classical $(\beta/\alpha)_8$ TIM barrel except that the barrel is composed of only seven strands. A long substrate binding groove extends across the C-terminal end of the barrel. Cocrystallization with a substrate analog revealed the presence of a HA tetramer bound to subsites −4 to −1 and distortion of the −1 sugar.

Conclusions: The structure of the complex strongly suggest an acid–base catalytic mechanism, in which Glu113 acts as the proton donor and the *N*-acetyl group of the substrate is the nucleophile. The location of the catalytic residues shows striking similarity to bacterial chitinase which also operates via a substrate-assisted mechanism.

Introduction

Hyaluronidases are widespread in nature, being found in mammals, insects, leeches, and bacteria [1, 2]. These enzymes hydrolyse hyaluronic acid (HA), a high molecular weight nonsulfated linear glycosaminoglycan, which is composed of repeating disaccharide units, D-glucuronic acid (GlcA), and *N*-acetyl glucosamine (GlcNAc). They also hydrolyse chondroitin sulfates and, to a small extent, dermatan sulfate. HA is found in almost all tissues and body fluids and is particularly abundant in the soft connective tissues of cartilage, synovial fluid, and the vitreous humor of the eye. In the extracellular matrix HA is a component of the ground substance that connects protein filaments, collagen fibers, and the connective tissue cells. The structural properties and biological role of HA are well studied [3, 4]. The structural role of HA as a stabilizer, lubricant, and shock absorbant is based on its viscoelastic properties, which are dependent on the concentration and molecular weight of HA. The level of HA is markedly elevated during embryogenesis, wound healing, malignant transformation,, and whenever fast tissue turnover and repair is required (see recent review by R Stern and TB Csóka, on mammalian hyaluronidases on the website http://www.glycoforum.gr.jp). In vertebrates, the turnover of HA is controlled by hyaluronidase, which is an endoglycosidase that acts jointly with two exoglycosidases, β-glucuronidase, and β-*N*-acetyl glucosaminidase. Hyaluronidase from bee venom (Hya) specifically degrades HA in the extracellular matrix of skin, thereby facilitating penetration of venom constituents into the body. Hya shares greater than 50% sequence identity with hyaluronidases from other hymenoptera [5] and, interestingly, also with several mammalian enzymes (as much as 30% identity). These include the sperm GPI-membrane-bound PH-20 protein [6], which is essential for fertilization, and the human lysosomal enzymes Hyal-1 [7] and Hyal-2 [8] that are involved in HA turnover (Figure 1). The best characterized enzymes are Hya [6, 9] and PH-20, which also catalyses the transglycosylation reaction [10, 11]. PH-20 protein, in the acrosomal membrane of the sperm, degrades the HA-rich matrix in which cumulus cells surrounding the egg are embedded, enabling sperm–egg adhesion. It has been shown that PH-20 is an effective antigen for immunocontraception [12]. On the basis of sequence similarity mammalian and insect hyaluronidases have been classified as belonging to family 56 of glycosyl hydrolases [13, 14].

Native Hya isolated from bee venom [9] is a single polypeptide composed of 350 residues. It is secreted as a basic glycoprotein with a carbohydrate content that accounts for 7% of the protein mass [9], and contains two disulfide bridges and four potential glycosylation sites (Asn–X–Thr, where X is any amino acid). Recombinant Hya has been expressed in prokaryotic (*Escherichia coli*) and eukaryotic (*Baculovirus*) hosts [15]. Although native-like enzymatic activity and IgE binding capacity were observed for the Baculovirus-expressed protein, markedly lower values were obtained with Hya expressed in *E. coli*.

Hya is an endo-*N*-acetyl-D-hexosaminidase that specifically cleaves the β-1,4 glycosidic bond between GlcNAc and GlcA of long HA chains. The end product of exhaustive hydrolysis is the tetrasaccharide GlcA–GlcNAc–GlcA–GlcNAc [10, 11]. The catalytic mechanism of Hya is unknown. However, the structures of other glycosyl hydrolases show usually at least two acidic residues in the active site. In lysozyme [16], chitinase [17], and cellobiohydrolase [18] these are aspartate and gluta-

To whom correspondence should be addressed (e-mail: zora.housley@unibas.ch).

Key words: allergen; bee venom; crystallography; glycosidase family 56; hyaluronidase

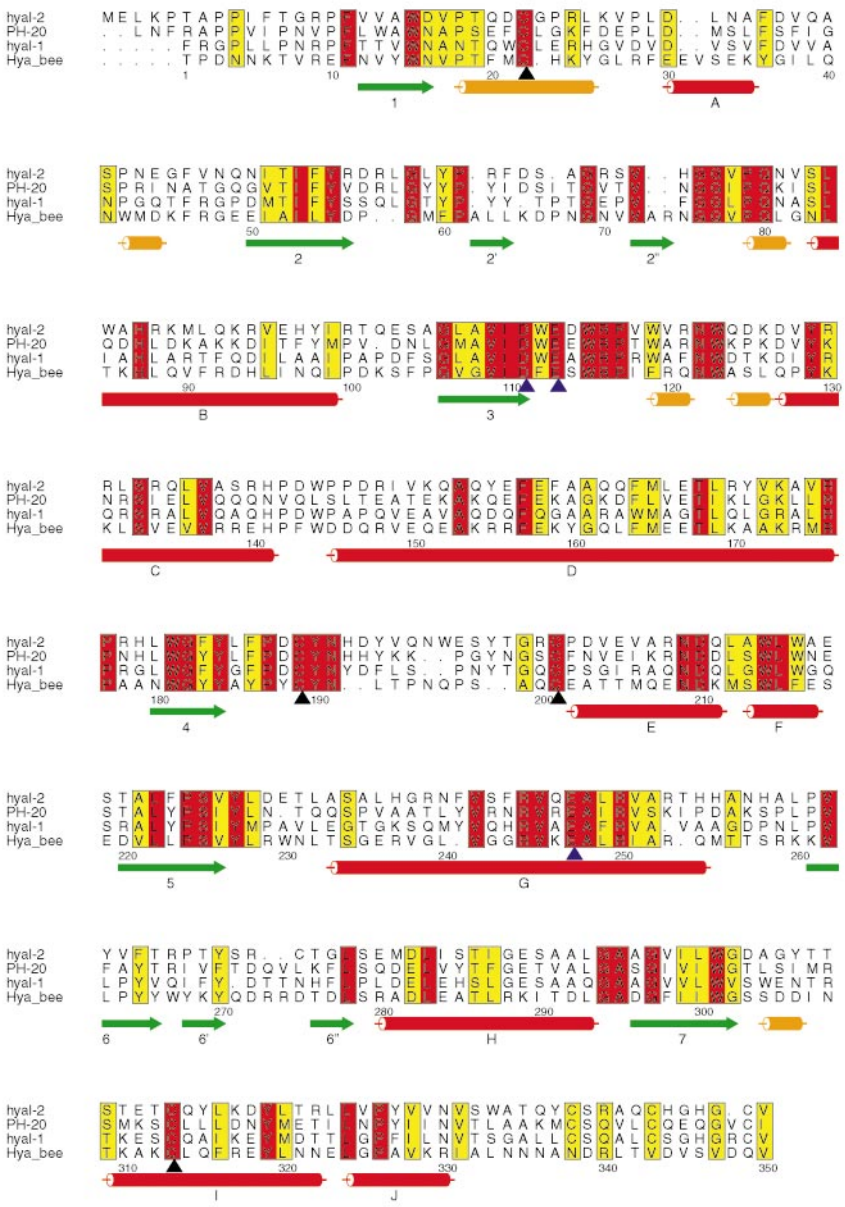

Figure 1. Sequence Alignment of Bee Venom Hya with Human Hyaluronidases

The proteins are listed from top to bottom: lysosomal hyaluronidase Hyal-2 (residues 1–355), sperm PH-20 protein (1–353), lysosomal hyaluronidase Hyal-1 (1–349), and bee venom Hya (entire sequence, residues 1–350). Fully conserved residues are shown in red, partially conserved residues in yellow. Secondary structure elements for Hya are shown below the sequences: green arrows represent β strands, red cylinders α helices, and orange cylinders 3_{10} helices. Blue arrowheads denote the active-site residues Asp111 and Glu113, as well as Glu247 of bee venom Hya. The four cysteine residues forming two disulfide bridges, Cys22–Cys313 and Cys189–Cys201, are marked by black arrowheads. The sequence of mature Hya starts with Thr (TPDN…), as determined by protein sequencing [70] (D Hoffman, personal communication), that is, one residue earlier than reported by Kreil and coworkers [6], based on nucleotide sequencing.

mate, whereas two glutamate residues are found in xylanase [19] and β-amylase [20, 21]. Of these, one carboxylate group functions as the acid/base catalyst and the other as the catalytic nucleophile [22]. The mechanism proceeds either via a double or a single nucleophilic substitution, resulting in retention or inversion of the configuration of the anomeric carbon, respectively. Some glycosidases that act on *N*-acetylglucosamine-containing saccharides, such as chitinolitic enzymes, lack the proteinaceous nucleophile and the *N*-acetyl group of the substrate acts as the nucleophilic base in a substrate-assisted reaction (see [23] and references therein). The active-site residues of Hya have not yet been identified. However, mutagenesis studies on the human sperm PH-20 protein suggested Asp111, Glu113, and Glu247 as candidates [24].

The venom of honey bee contains proteins that can induce life-threatening allergic reactions in humans [25]. It has been shown that Hya and phospholipase A2 are the major allergens because they can induce pathogenic reactions in the majority of patients allergic to bee venom (71% of patients had specific serum IgE to recombinant Hya and 78% to recombinant phospholipase A2 [26]). Nonallergic control individuals had no IgE antibodies to either of the two recombinant enzymes whereas 15% showed some IgE antibodies to whole bee venom, indicating a superior diagnostic specificity of recombinant allergens compared to whole bee venom. The allergic response is initiated by allergens that cross-link the Fc-receptor-bound IgE antibodies on the surface of mast cells. This is followed by rupture of the mast cell membrane and the release of stored mediators, such as histamine, which are responsible for the immediate hypersensitive reaction. A promising approach to inhibit the onset of allergy would be to prevent allergen binding to IgE. Knowledge of the molecular interactions between the allergen and the IgE antibodies may be obtained from structural studies combined with biochemical and immunochemical

Table 1. Diffraction Data and Phasing

	Monoclinic Form				Trigonal Form	
Data Set	Native-1	Native-2	$Pb(CH3COO)_2$	$PtCl_4$	Native	Complex
X-ray source	Rot. anode	Synchrotron	Rot. anode	Rot. anode	Synchrotron	Rot. anode
Temperature (°C)	4	−173	4	4	20	4
Resolution range (Å)						
Total	25–2.7	25–1.6	24–2.8	26–4.0	29.1–2.1	30–2.65
Outer shell	2.85–2.7	1.69–1.60	2.95–2.80	4.22–4.00	2.2–2.1	2.79–2.65
Unique reflections	9664	43,930	9041	2975	23,113	13,411
Completeness (%)[a]	95.4 (95.3)	96.3 (88.0)	99.4 (99.5)	95.4 (92.5)	87.5 (62.5)	99.8 (99.9)
Multiplicity[a]	3.1 (3.1)	2.3 (1.7)	3.1 (3.1)	2.8 (2.7)	1.8 (1.7)	3.7 (3.7)
Intensity ($I/\sigma(I)$)[a]	7.6 (2.3)	8.2 (2.6)	7.8 (3.4)	6.3 (4.8)	5.0 (1.9)	7.4 (2.6)
R_{merge} (%)[a]	9.4 (33.0)	3.8 (25.1)	7.9 (20.1)	10.4 (14.6)	11.1 (32.6)	10.0 (29.5)
R_{iso} (%)[b]			19.1	29.0		
R_{Cullis}[c] (centric/acentric) (%)			73/68	80/86		
Phasing power[d]			1.36/1.80	1.60/1.40		

[a] Values in parentheses refer to the highest resolution shell.
[b] $R_{iso} = \Sigma||F_{PH}| - |F_p|\Sigma|F_p|$, where F_p and F_{PH} are the structure factors of native and derivative crystals.
[c] $R_{Cullis} = \langle$lack of closure$\rangle/\langle$isomorphous difference$\rangle$.
[d] Phasing power $= \langle F_H/$lack of closure$\rangle$.
Crystals of the monoclinic form are in space group $P2_1$ with unit-cell dimensions a = 39.9 Å, b = 90.2 Å, c = 49.1 Å, β = 92.4°; crystals of the triclinic form are in space group $P3_221$ with unit-cell dimensions a = 71.2 Å, b = 71.2 Å, c = 152.1 Å. All data sets were collected from one crystal each on MAR-research image-plate detectors.

characterization. Such information might provide the basis for the development of allergen-specific forms of therapy.

The X-ray structure of hyaluronidase from bee venom, determined in two different crystal forms and in complex with an HA oligomer, provides insight into the mode of substrate binding and the catalytic mechanism. The structure of Hya will be used to model the sequence-related mammalian enzymes and, hopefully, will lead to identification of the mechanism that triggers the allergic response caused by the sting of the honey bee.

Results and Discussion

Structure Determination

Two crystal forms of Hya, monoclinic and trigonal, were used for the structure determination. Two heavy-atom derivatives were found for the monoclinic form (Table 1). The resulting multiple isomorphous replacement (MIR) map at 2.7 Å resolution was rather poor, but allowed the building of a partial model. For phase improvement multi-crystal averaging was employed. For this, the experimental electron density corresponding to one molecule was transferred into a large P1 cell employing a mask based on the partial model. The derived structure factors were used for molecular replacement to solve the trigonal crystal form. An outstanding solution with an R factor of 42% was found. Cyclic electron-density averaging between the two crystal forms to 2.7 Å resolution resulted in a markedly improved map. Finally, after tracing most of the chain in the monoclinic form, the model was subjected to conventional refinement using the high-resolution synchrotron data set to 1.6 Å resolution (Table 2). The final model consists of residues 10–330. The conformations of the nine N-terminal and the 20 C-terminal residues (plus the His_6 tail) are not defined by electron density. In addition, density is missing for loop segments comprising residues 65–71, 193, 194, and 255–259. The model shows good stereochemistry and has a free R factor of 22.7% (Table 2). An example of the final $2F_o–F_c$ map is shown in Figure 2.

Overall Fold and Structure Comparison

Hya is a globular single-domain protein with approximate core dimensions 52 × 44 × 39 Å. It comprises ten α helices, 11 β strands, six 3_{10} helices (one comprising seven residues and the others three residues each; Figure 3). The overall fold (Figures 3 and 4) resembles that of a classical $(\beta/\alpha)_8$ TIM barrel [27], which is common to many hydrolases [28]. However, in Hya only seven strands (β1–β7) form the barrel that is surrounded by α helices A–J. There is a lack of closure between strands β1 and β2, which do not interact through hydrogen bonding, leaving a wide gap (7–8 Å) that could accommodate an additional strand (Figure 3). Loop 34–49 partly fills this gap with two polar mainchain atoms of Leu39 engaged in parallel β sheet hydrogen-bonding interactions with the mainchain atoms of Val13 and Trp15 of β1. Other unusual features, that deviate from the regular $(\beta/\alpha)_8$ barrel, are the presence of two α helices between strands 3 and 4 (helices C and D) and 4 and 5 (helices E and F) and two β hairpins comprising residues 63–75 and 269–279 at the C-terminal end of β2 and β6, respectively. Hya contains two disulfide bridges (Figure 3b). The first, Cys189–Cys201, stabilizes the base of a long loop at the C-terminal

Table 2. Refinement

Space Group	$P2_1$	$P3_221$	$P3_221$
Data set	Native	Native	Complex
Resolution range (Å)	8.0–1.6	8.0–2.1	8.0–2.65
Total No. of reflections	43,540	23,578	12,837
R factor[a] (R_{free}) (%)	18.5 (22.7)	20.0 (25.7)	16.3 (25.2)
No. of protein atoms	2609	2681	2681
No. of water molecules	354	203	132
No. of ligand molecules			53
Rmsd from ideal values			
Bond lengths (Å)	0.007	0.008	0.009
Bond angles (Å)	0.022	0.028	0.032
Average B factor ($Å^2$)			
Protein atoms	21.6	21.5	34.3
Solvent atoms	35.4	49.6	38.4
Ligand atoms			39.0
Rms ΔB ($Å^2$)			
Mainchain bond	2.5	2.6	3.1
Sidechain bond	4.3	3.5	4.4

[a] R factor is the conventional R factor and R_{free} is the R factor calculated with 10% of the data that were not used for refinement.

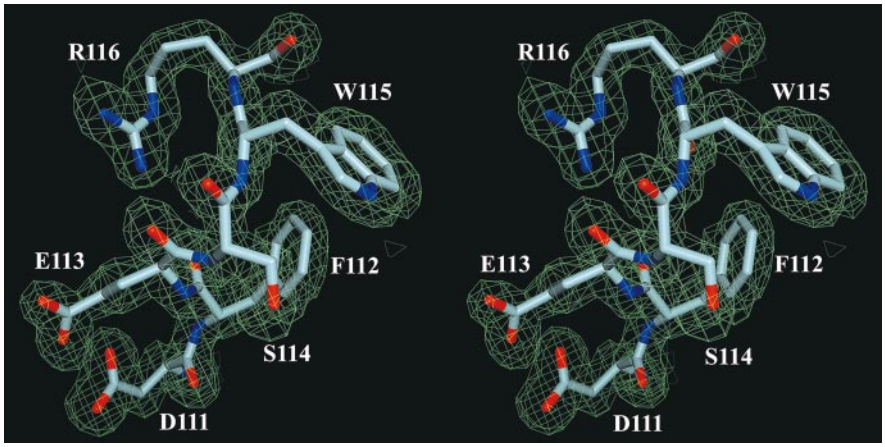

Figure 2. Representative Section of the Final Electron Density Map

Close-up stereo view of the segment 111–116, including the proton donor Glu113, overlaid onto the final SigmaA-weighted $2F_o–F_c$ map [71] contoured at 1σ. Figures 2, 3, and 5–7 were produced using the program DINO (A. Philippsen, http://www.biozentrum.unibas.ch/~xray/dino).

end of β4, whereas the Cys22–Cys313 bridge joins distant secondary structure elements, a 3_{10} helix near the N terminus and α helix I near the C terminus. The Hya sequence contains four potential glycosylation motifs (Asn–X–Thr) at asparagine residues 4, 83, 191, and 231. Asn191 and Asn231 can be ruled out as glycosylation sites because they are buried in the protein. The N terminus including Asn4 is not defined by electron density, whereas weak electron density extends from Asn83, corresponding to two sugar residues.

Another seven-stranded 'open' barrel has been observed in the structure of quinolinic acid phosphoribosyltransferase (QAPRTase) [29]. Here, the gap that occurs between strands 2 and 3 is partially occupied by the substrate. In Hya there are no hydrogen bonds between strands 1 and 2 whereas in QAPRTase the analogous strands interact through a single hydrogen bond. Seven-stranded β/α barrels with equally spaced strands have been reported for cellobiohydrolase II [30] and the related thermophilic endocellulase E2 [31].

A search for proteins with a similar fold was performed using the Dali [32] server. The top scoring proteins were all glycosidases with a regular $(\beta/\alpha)_8$ barrel fold (Table 3), with the exception of the seven-stranded barrel of thermophilic endocellulase E2 [31]. The observed similarity is mainly confined to the β barrel and the surrounding α helices, with the β strands in register (i.e., the first strand of Hya being structurally equivalent with the first strand of the corresponding protein, etc.). The seven-stranded β barrel of endocellulase with evenly spaced strands, however, does not fit the 'open' Hya barrel closely. Significant similarity in the active-site region (see below) was only observed for bacterial chitinase A [17], which showed a somewhat lower overall score ($Z = 9.2$), but had similar locations for the catalytic residues and for several conserved aromatic residues in the binding cleft (data not shown).

The Substrate Binding Groove

The dominant feature of the Hya protein surface is a large groove that extends perpendicularly to the barrel axis, approximately from strand 1 to strands 4 and 5 (Figure 5). Loops following β strands 2, 3, and 4 form one wall of the groove and those following 1, 5, 6, and 7 the other. The size of the groove is $\sim$30 Å $\times$ 10 Å and would be large enough to accommodate a hexasaccharide. This is consistent with solution binding studies on the testicular enzyme which showed that $(GlcA–GlcNAc)_3$ is the smallest oligomer that can be hydrolysed [10, 11]. Most residues in the groove are conserved between insect and mammalian hyaluronidases as shown in Figure 5b. Grooves of similar shape have been found in several endoglycosidases where they form the binding site for long polysaccharide substrates [16, 19, 31]. In Hya, a number of conserved residues (Asp111, Glu113, Arg116, Arg244, Tyr55, Trp123, Tyr184, Tyr190, Tyr227, Tyr265, Trp301, and Ser225) line the groove (Figure 6). A large number of aromatic residues are observed, reminiscent of other sugar binding proteins. The two conserved arginines observed at the opposite walls of the binding groove, probably guide the substrate into the active site through electrostatic interactions with the carboxylic groups of hyaluronic acid. Many of the conserved active-site residues are located in the long loops adjacent to β strands 3 and 4 comprising residues 111–124 and 184–201, respectively (Figure 6). The hydrophilic loop 65–71 (KDPNGNV) joining the β strands of the hairpin 62–74, located above the active site, is not visible in the electron-density map of the monoclinic crystal form. It is, however, fully defined in the trigonal form, where it is stabilized by crystal contacts and is located far from the active site.

Structure of the Enzyme–Hyaluronic Acid Tetramer Complex

Hya was cocrystallized in the presence of a HA-hexamer $(GlcA–GlcNAc)_3$, modified with a fluoresceinamine group at C1 of the reducing sugar (see the Experimental Procedures section). The structure was solved to 2.65 Å resolution in the trigonal form (Tables 1 and 2). Electron density accounting only for a $(GlcA–GlcNAc)_2$ fragment was observed in the substrate binding groove (Figure 7), with the reducing end oriented close to the putative proton donor Glu113 (see below). Thus, the tetrasaccharide most probably represents a cleavage product that is bound to subsites -4 to -1, according to the nomenclature for sugar binding subsites in glycosyl hydrolases [33] (–n is a subsite at the nonreducing end and $+$n at the reducing end, with cleavage taking place between sugars in the -1 and $+1$ subsites). The bound tetrasaccharide is formed by the removal of a disaccharide from the reducing end of the fluorosceinated hexasaccharide. In contrast, Takagaki et al. [11] reported that a HA hexamer labeled at the reducing end with 2-aminopyridine was not digested by sperm PH-20 protein following 3–4 hr of incubation, whereas higher oligomers were hydrolyzed by successive removal of GlcA–GlcNAc dimers from the nonreducing end. Degradation observed in our study might be due to the long time required for crystallization of the complex (three months).

Although the saccharide in subsite -4 appears loosely bound

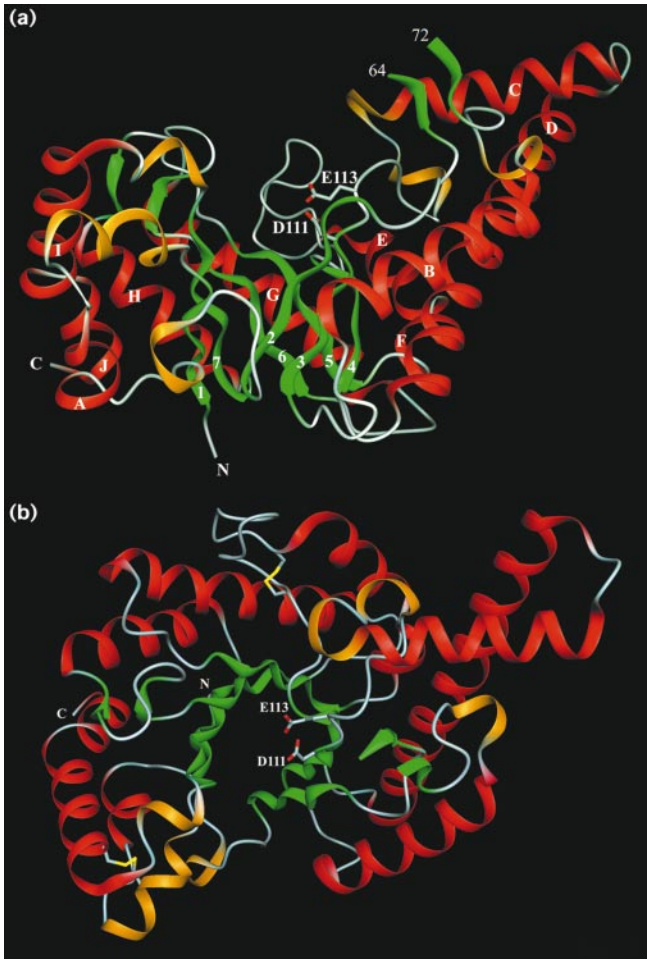

Figure 3. Ribbon Representation of the Crystal Structure of Hya

α Helices are colored in red, 3_{10} helices in orange, and β strands in green. (a) Side view of the barrel formed by β strands 1–7 (green arrows) and ten α helices marked A–J (red spirals) on the outside of the barrel. The barrel comprises residues 12–16 (strand 1), 50–56 (strands 2), 106–111 (strand 3), 180–184 (strand 4), 220–226 (strand 5), 261–268 (strand 6), and 296–302 (strand 7). The substrate binding groove is located at the C-terminal end of the β barrel (top). Asp111 and Glu113 are shown as stick models.

(b) View along the barrel axis, that is, after rotation by 90° around a horizontal axis. The two disulfide bridges are in yellow.

to the protein, the *N*-acetyl group of sugar residue −3 and the carboxylate group of −2 are hydrogen bonded to the hydroxyl groups of nonconserved Ser304 and Ser303, respectively (Figure 7). In addition, the carboxylate of sugar residue −2 interacts with the mainchain amide of residue 304 and stacks with its sugar ring against Tyr55. The *N*-acetyl group of GlcNAc in the −1 subsite is deeply buried in a pocket with its carbonyl and amide groups hydrogen bonded to the sidechains of Tyr227 and Asp111, respectively. The chair conformation is observed for the saccharides bound in subsites −2, −3, and −4, whereas the boat conformation is adopted by GlcNAc in subsite −1. GlcNAc in subsite −1 lacks density for the C6–O6 sidechain and exhibits weak density for C5 and O1. This may indicate partial disorder due to fewer stabilizing interactions after cleavage.

Catalytic Groups and Reaction Mechanism

Two acidic residues constitute the catalytic site in most glycosidases, one acting as the proton donor and the other as the nucleophile. The only carboxylic residues present in the Hya binding groove are the strictly conserved Asp111 and Glu113 residues (Figure 1) which protrude from the C-terminal end of β3 (Figure 3). Glu113 appears well positioned to act as the proton donor with a distance of 2.6 Å between its sidechain carboxylate and the glycosidic oxygen (Figure 7a). In contrast, the carboxylate oxygens of Asp111 are separated by more than 5 Å from the glycosidic oxygen. Indeed, functional analysis of respective mutants in the related human sperm PH-20 protein indicated that Glu113 is more important for catalysis than Asp111. Replacement of Glu113 by glutamine and Asp111 by asparagine in PH-20 (equivalent to Glu113 and Asp111 in Hya) resulted in a protein with no detectable activity and 3% activity, respectively [24]. This, together with the crystal structure, suggests direct involvement of these residues in catalysis. Interestingly, the glutamic acid was also identified as the proton donor in the structurally equivalent carboxylic pairs in endo-β-*N*-acetylglycosaminidase H (endo H) [34, 35] (Asp130–Glu132), hevamine [36] (Asp125–Glu127), and chitinase A from *Serratia marcescens* [23] (Asp313–Glu315). The impaired function of the three other PH-20 mutants (Glu249 → Gln, Arg252→Thr, Arg176→Gly), investigated in the same study, is probably caused by structural perturbations. Glu249 and Arg252 correspond to Glu247 and Arg250 in Hya (Figure 1), where they form an intrahelical (helix G) salt bridge that is partly buried by the adjacent helix E. Although this salt bridge is too far away from the putative active site for direct involvement in catalysis (Figure 6), its disruption may destabilize the entire structure. The other mutated residue, Arg176 (the equivalent of Arg176 in PH-20), is also not part of the binding groove, but is buried between helices B and D with its guanidinium moiety bound to mainchain carbonyl groups of both helices. It is interesting to note that nonconservative mutation of Glu268 to lysine in Hyal-1, which corresponds to Glu247 in Hya, was identified in a patient deficient in serum hyaluronidase. This disorder is known as mucopolysaccharidosis IX [37].

The carboxylate of Glu113 forms a short hydrogen bond with Asp111 (Figures 6 and 7). In the unliganded structure, the sidechains of these putative catalytic residues are partly solvent exposed. They are bound to three water molecules (not shown) but make no further protein contacts. The average distance between the four carboxyl oxygens of the two carboxylates is 3.8 Å, considerably shorter than the 5.5 Å found in retaining glycosidases [38]. Atoms Glu113 Oδ2 and Asp111 Oδ1 are separated from each other by 2.5 Å and have the right geometry for hydrogen-bond formation (angles 111Cγ–111Oδ1–113Oϵ2 and 111Oδ1–113Oϵ2–113Cδ are 117° and 118°, respectively). For steric reasons the two carboxylates cannot approach the anomeric carbon of the substrate from opposite sides, as observed in many retaining glycosidases. The close interaction between the two carboxylic acids was observed in the monoclinic and trigonal crystal forms grown at pH 4.2 and 6.5, respectively, as well as in the liganded structure at pH 6.5. The close proximity of the two COO− groups should result in elevated pK values and protonation of one of the sidechain carboxylates. Short hydrogen bonds between carboxylates have been observed in the active sites of diverse enzymes and are either buried in the protein ('low-barrier hydrogen bonds', described by Cleland and Kreevoy [39]), or exposed to the solvent as for the periplasmic glucose/galactose binding protein [40] and, more relevant, in the glycosidases cellobiohydrolase II [30, 41], endo-β-*N*-acetylglycosaminidase F1 [42] (endo F1), hevamine [36], and chitinase A1 from *Bacillus circulans* [43]. It was proposed that interactions with ordered water molecules

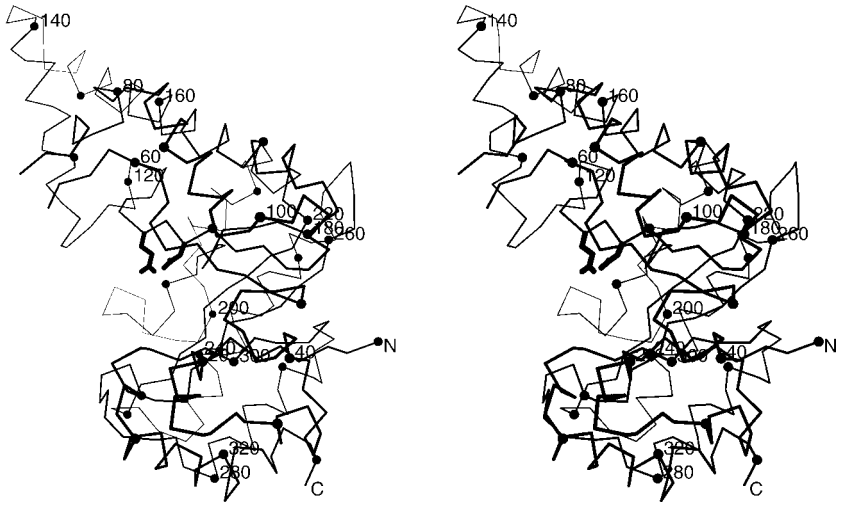

Figure 4. Stereo Cα Trace of the Hya Molecule

The view is rotated by 90° around an axis perpendicular to the paper with respect to the view in Figure 3a. Every tenth residue is highlighted with a black circle and every twentieth residue is labeled.

stabilize the short hydrogen bond [44]. Accordingly, substrate binding will disorder the solvent network and facilitate the uptake of a proton by the substrate.

As in Hya, there is no obvious proteinaceous nucleophile in several other retaining β-1,4-glycosidases which act on GlcNAc in the −1 position, such as hevamine, chitinase, and chitobiase (see [23] and references therein). In these enzymes, the nucleophilic function is performed by the carbonyl oxygen of the substrate's *N*-acetyl group at C2 [23, 36]. The prerequisite for this substrate-assisted reaction is the accurate positioning of the *N*-acetyl sidechain of the substrate with respect to the enzyme. The reaction can then proceed either via a positively charged oxocarbonium ion intermediate or an oxozolinium ion with a covalent bond between the *N*-acetyl carbonyl oxygen and the C1 atom [23].

In Hya, as well as in the chitinolytic enzymes, the position of the *N*-acetyl sidechain is tightly defined by two hydrogen-bonding interactions: one between its amide NH and Asp111, and the other between its carbonyl oxygen and the hydroxyl group of the conserved Tyr227. Furthermore, the methyl group of the *N*-acetyl sidechain forms hydrophobic interactions with Tyr184 and Trp301 (Figure 7a). Similar interactions have been observed in the liganded structures of chitobiase [45] and hevamine [23], where the corresponding residues are Asp539, Tyr669, Trp616, and Trp639 and Asp125, Tyr183, and Tyr6, respectively. In Hya, the tight interaction of the N-acetyl group with the surrounding protein groups requires deformation of the sugar ring −1 from the $^4C_1$ chair to the $^{4,1}C$ boat conformation (Figure 7b). The carbonyl group of the *N*-acetyl moiety points toward C1 of the −1 sugar ring with a O7–C1 distance of 2.9 Å (Figure 7b), which compares well with the corresponding distances of 3.0 Å for chitobiase and 2.8 Å for hevamine. At this close distance, the partial negative charge of the carbonyl oxygen is well positioned to stabilize the positive charge of the anomeric carbon, as postulated for the oxocarbonium ion intermediate. This distortion, induced by binding into the active site, facilitates the reaction by bringing the glycosidic bond into a near equatorial position and moving the glycosidic oxygen nearer to Glu113, the proton donor [46]. Clearly, Hya belongs to the group of retaining enzymes, because the anomeric C1 is found in a β configuration in the enzyme–HA-tetramer complex. Distortion of the pyranoside ring bound at site −1 was first observed for planar oxocarbonium ion intermediate in lysozyme [47]. Half-chair conformations were observed in the enzyme–product complexes of hen egg white lysozyme [48, 49] and bacteriophage T4 lysozyme [50]. Twisted boat conformations, in which C1, C2, C3, C5, and O5 atoms are nearly coplanar, were found in chitobiase complexed with uncleaved dichitobiose in the active site [45] and in the crystal structure of the retaining β-endoglucanase I in complex with a nonhydrolysable substrate analog [51]. Distortion of the glycosyl unit in the −1 site from the usual chair to the ^2S_O conformation has recently been reported for cellobiohydrolase (Cel6A) in complex with nonhydrolysable cello-oligosaccharide [41].

In conclusion, Hya is a retaining β-glycosyl hydrolase that catalyzes an acid/base reaction mechanism with Glu113 acting as the proton donor and the *N*-acetyl carbonyl group of the substrate acting as the nucleophilic base. Assignment of the conserved Glu113 as catalytic residue is in agreement with mutagenesis studies on the sequence-related human sperm

Table 3. Structural Similarity of Hya with Other Proteins

Protein	PDB Code	Family	Z Score[a]	Rmsd (Å)	Cα Atoms	Reference
β-Amylase (*Bacillus cereus*)	1b9z	14	12.3	2.2	115	[21]
β-Amylase (Soybean)	1byb	14	11.5	2.3	133	[20]
β-Glucuronidase	1bhg	2	11.5	2.3	154	[73]
Myrosinase	2myr	1	11.4	2.3	128	[74]
Endo-β-xylanase	1tax	10	11.0	2.1	130	[75]
Thermophilic endocellulase E2	1tml	6	9.9	2.2	134	[31]
Bacterial chitinase A	1ctn	18	9.2	2.3	108	[17]

[a] As defined in the program DALI [32]. Several entries between 1tml and 1ctn have been omitted for convenience.

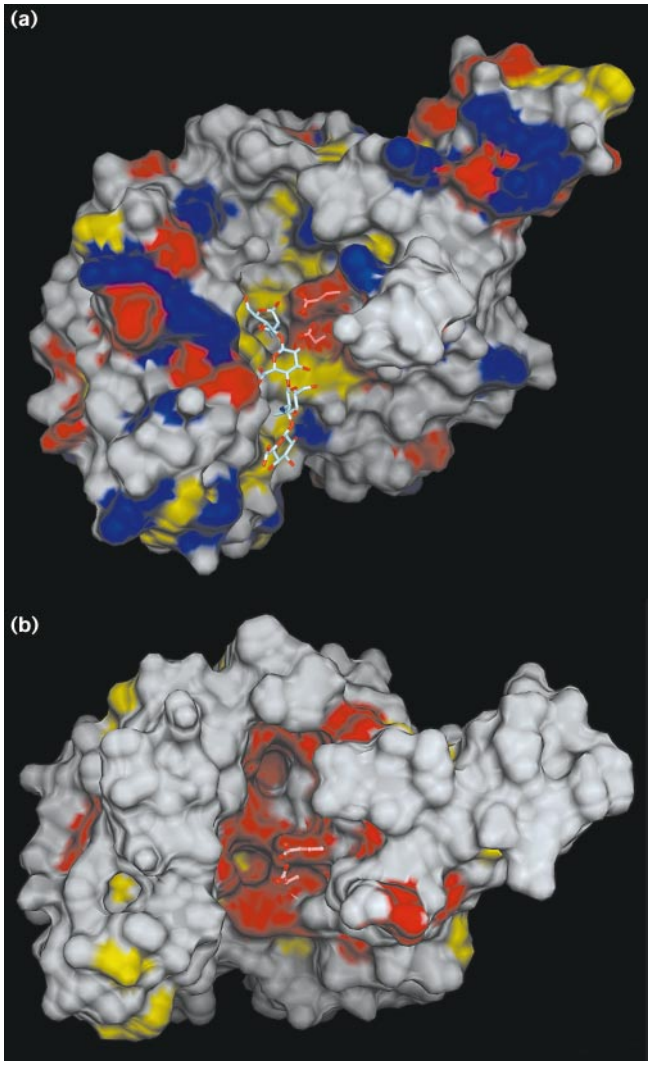

Figure 5. The Molecular Surface of Hya Viewed as in Figure 3b

(a) The surface is color coded according to residue type with red, blue, and yellow representing acidic, basic and aromatic residues, respectively. The $(GlcA–GlcNAc)_2$ tetramer bound to the substrate binding groove and residues Asp111 and Glu113 are shown as stick models.

(b) Mapping of conserved residues onto the Hya molecular surface. Red denotes residues that are identical in all four sequences shown in Figure 1; yellow denotes similar residues.

PH-20 protein. Moreover, a multiple sequence alignment of bee venom hyaluronidase with human hyaluronidases, belonging to family 56 glycosidases, indicates conservation of the active-site residues, suggesting a similar catalytic mechanism for the mammalian enzymes.

Allergenicity

Hya is a major allergen of bee venom that can induce serious, occasionally fatal, systemic IgE-mediated anaphylactic reactions in human [25]. Only a few three-dimensional structures of allergens are known to date, four from plants and five from animals (see [52] and references therein) [53]. These structures are different from the $(\beta/\alpha)_7$ barrel fold of Hya. Mammalian lipocalins [52, 53] show an antiparallel β barrel fold as does the plant allergen Phl p 2 from timothy grass [54]. Profilin allergens [55, 56] have a large β sheet with flanking helices, and the major mite allergen Der f 2 [57] resembles immunoglobulin. Thus, no unique structural feature responsible for the allergenicity can be identified. However, Rouvinen et al. [52] pointed out that all these proteins are monomers (except for the dimeric major horse allergen [53]) of similar dimensions. This also applies to Hya.

Antigenicity of Hya is fully determined by the structure of its epitopes, the areas of the protein surface that are recognized by specific antibodies. The structure of the Hya surface, which is now known in full detail, contains an unusually high number of charged residues which are evenly distributed on the surface (Figure 5a). Of all surface residues, 41% comprise aspartate, glutamate, lysine or arginine residues. This is considerably higher than the average value of 27% [58]. Although some of these residues may now be subjected to mutagenesis, the identification of the Hya epitope(s) must await further studies. The full characterization of the antigen–antibody recognition sites will require the elucidation of the structure of complexes between Hya and Fab fragments (from various mAb against Hya), because epitopes are generally composed of a discontinuous array of amino acids [59]. Site-directed mutagenesis of epitope residues may lead to mutant variants with low IgE binding activity (hypoallergens) [60] which might be used in immunotherapy without the risk of side effects. An example of this approach is a six-point mutant of Bet v 1, the major allergen of birch pollen, which exhibits extremely low reactivity with serum IgE from birch pollen-allergic patients [60].

Biological Implications

Hyaluronidases are a group of hydrolytic enzymes which degrade hyaluronic acid (HA), a high molecular weight polysaccharide found in virtually all mammalian tissues and body fluids. HA is a ubiquitous component of the vertebrate extracellular matrix where it fills the space between cells and fibers and acts as a lubricant as well as a barrier to penetration by foreign particles. HA levels are markedly increased during embryogenesis, inflammation, malignant transformation, wound healing, and whenever fast tissue turnover and remodeling is required. Defects in HA metabolism appear to be related to various diseases suggesting that the level of HA must be tightly controlled. Surprisingly, the study of the enzymes involved in HA synthesis and degradation has been greatly neglected.

The 1.6 Å resolution crystal structure of hyaluronidase, a major allergen from bee venom, gives insights into the mode of substrate binding and the substrate-assisted catalytic mechanism. It also represents the first step toward the elucidation of a Hya–antibody complex structure which is needed to identify the Hya epitope(s). Susceptible individuals respond to exposure with Hya by producing IgE antibodies which, following reexposure, bind to the allergen and thus induce an anaphylactic reaction. Nonallergic individuals (e.g., beekeepers) produce mainly IgG4 antibodies associated with an immunoprotective role. Knowledge of the structure of the Hya epitopes will provide a basis for understanding its allergenicity and is expected to have a strong impact on the treatment of Hya-induced allergy. Rationally designed ligands that can compete with IgE antibodies for the allergen binding site could prevent the allergen-induced release of mediators from effector cells. Alternatively, mutant proteins that bind weakly to IgE antibodies but can still interact with allergen-specific T cells could be used for immunotherapy to suppress IgE sensitization to Hya, with-

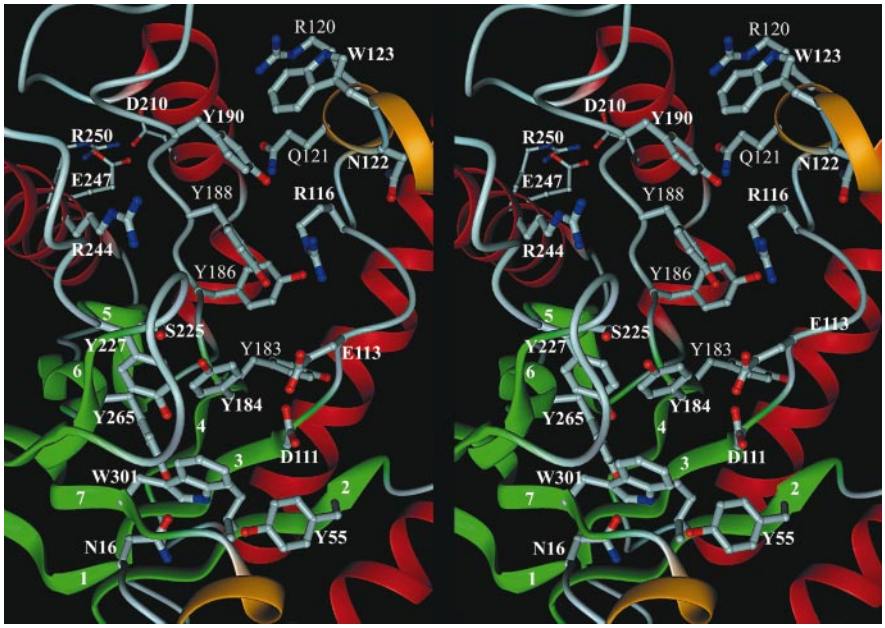

Figure 6. The Substrate Binding Groove

Stereoscopic close-up view of the groove extending across the C-terminal end of the β barrel (green arrows). Bold labels indicate conserved residues (Figure 1).

out risk of side effects. This T cell targeted therapeutic approach will hopefully result in the induction of allergen-specific immune tolerance.

Hya is closely related to the human PH-20 sperm protein, which enables sperm–egg adhesion, and human plasma hyaluronidases involved in HA turnover, the malfunctioning of which is related to various diseases. For example, the synovial fluid of joints in patients suffering from osteoarthritis and rheumatoid arthritis has increased hyaluronidase activity that results in a decrease of HA size and concentration. Interestingly, increased expression of a hyaluronidase similar to PH-20 has been found in tumor cells [61]. There, the enzyme is used to break down the basement membrane and facilitates tumor invasion, angiogenesis, and metastasis. With the knowledge of the Hya structure, modeling of the human enzymes should now be feasible. These structures will enable the rational design of specific inhibitors which could be used to combat hyaluronidase-related disorders.

Experimental Procedures

Purification

Recombinant enzymatically active Hya, containing a C-terminal His_6 tag, was produced by *Baculovirus*-infected insect cells and purified by Ni^{2+}-chelate chromatography, as described previously [15]. For crystallization experiments the protein was dialyzed against 5 mM sodium acetate buffer (pH 5.4) and concentrated to 8–10 mg ml^{-1}.

Synthesis of the Fluoresceinated Oligomer

The HA hexamer (150 mg) was dissolved in a 1 M sodium cyanoborohydride (Aldrich) solution in 30% AcOH/DMSO (3 ml) and fluoresceinamine (130 mg) was added (Aldrich). After heating the mixture at 90°C for 3 hr, the reaction was stopped by adding an equal volume of methanol. The product was precipitated from acetone and filtered. The solid material was recrystallized from acetonitrile and vacuum dried. Filtered supernatant, containing fluoresceinated oligomer, was concentrated and further purified by gel-filtration chromatography (Sephadex G-10 column). The total yield of fluoresceinated oligomer was 48%. The identity and purity of the final compound was determined by TLC (RP-18, eluent acetonitrile-water 8:2) and NMR analysis (Bruker AC200 200 MHz spectrometer).

Crystallization and Data Collection

Two crystal forms suitable for X-ray analysis were obtained by the hanging-drop vapour diffusion method at 20°C (Table 1). Trigonal crystals were obtained by mixing equal volumes of protein solution and 30% PEG 8000, 0.1 M Na-cacodylate (pH 6.5), 0.2 M ammonium sulfate and equilibrating over the latter solution. Crystals (0.3 × 0.5 × 0.2 mm) grew within 6–8 months and contained one molecule in the asymmetric unit, resulting in a solvent content of 54% (Vm = 2.7 $Å^3$/Da). Monoclinic crystals were obtained by mixing the protein (1:1) with 10% PEG 6000, 1.0 M NaCl, 20 mM acetic acid (pH 4.2) and equilibrating over the same solution. Crystals grew in several days to a typical size of 0.2 × 0.4 × 0.2 mm. There is one monomer per asymmetric unit and a solvent content of 47% (Vm = 2.3 $Å^3$/Da).

Prior to data collection, crystals were transferred into stabilizing solutions: 33% PEG 8000, 0.1 M Na-cacodylate (pH 6.5), 0.2 M ammonium sulfate for the trigonal crystals and 12% PEG 6000, 1.0 M NaCl, 5 mM Na-acetate (pH 4.4) for the monoclinic crystals. Derivative crystals were obtained by soaking native monoclinic crystals in stabilizing solutions containing heavy-atom compounds. Medium-resolution native and heavy-atom derivative data were collected in-house, at 4°C, on a MAR image plate area detector. For high resolution data collection, monoclinic crystals were flashed-cooled to 120K in a cryosolvent containing stabilizing solution plus 10% ethylene glycol. X-ray data were collected (native-2, Table 1) at the synchrotron radiation source at EMBL/DESY, Hamburg. High-resolution data of native trigonal crystals (Table 1) were collected at room temperature at the Daresbury (UK) synchrotron radiation source. Image data were indexed and integrated using MOSFLM [62]. The data were reduced and scaled using programs of the CCP4 package [63].

Structure Determination and Refinement of the Monoclinic Form

The structure was solved by MIR at 2.7 Å using phase information from two heavy-atom derivatives: $Pb(CH_3COO)_2$ (3 mM, two weeks soak) and $PtCl_4$ (1 mM, 24 hr soak). Derivative and native monoclinic data (native-1, Table 1) sets were scaled with program SCALEIT. The major lead and platinum sites were easily identified using isomorphous difference Patterson maps. Refinement of the heavy-atom parameters and calculation of initial phases were performed with the program MLPHARE [63] yielding a rather poor figure of merit of 0.36. Additional sites were identified by difference Fourier techniques. Final refinement of the heavy-atom parameters and phase calculation was done with the program SHARP [64] using data between 15 and 2.7 Å. Three binding sites for each of two derivatives were identified. Phase improvement was achieved by solvent flattening using the anticipated solvent content of 47% (SOLOMON [65]). The resulting map at 2.7 Å resolution was of sufficient quality to reveal α helices and β strands. A partial polyalanine model was built into regions of well-defined density with the aid of the

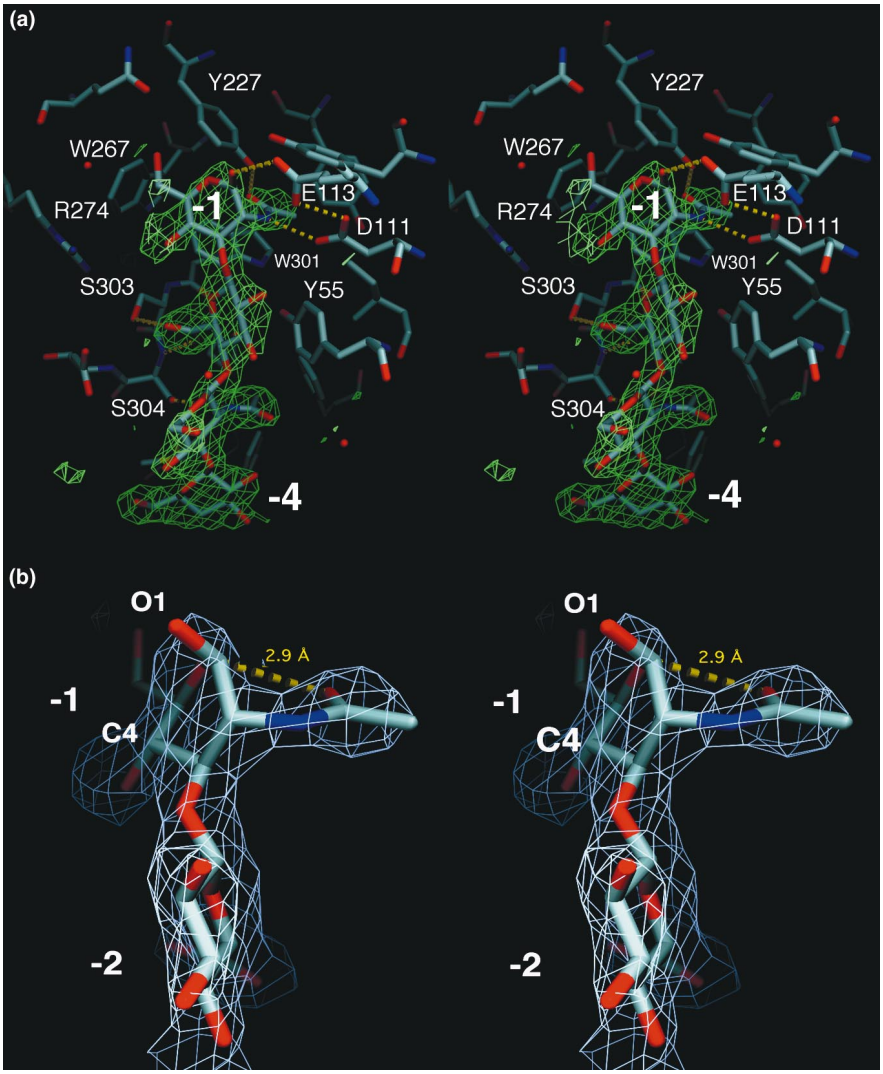

Figure 7. Stereoviews of the HA Tetramer GlcA-GlcNAc-GlcA-GlcNAc Bound to Hya

SigmaA-weighted simulated annealing [72] F_o–F_c electron-density map (contour level 3σ) has been calculated with the ligand omitted.
(a) The atomic model of the tetrasaccharide and of all protein residues within a distance of 5 Å to the sugar are shown. The reducing end of the tetrasaccharide (sugar residue −1) is at the top, close to Glu113. The view is similar to that in Figure 6.
(b) Close-up view of the distorted sugar ring of the GlcNAc residue in position −1. The view is rotated by about 90° around the vertical axis with respect to the view in (a).

BONES options in O [66]. The electron-density map, however, was not of sufficient quality to complete the model. The structure was eventually solved by multicrystal averaging (DMMULTI [67]) of the phased $P2_1$ and the unphased P_3221 crystal form, each having one monomer per asymmetric unit. The rotation/translation relationship between the molecules of the two crystal forms was determined by molecular replacement (AMoRe [68]), using the MIR density of the monoclinic form.

Initial refinement of the monoclinic form was carried out by REFMAC [63] using data set native-1. After manual adjustment of the model as indicated by sigma-weighted $2F_o$–F_c and F_o–F_c difference maps, refinement was continued using the high-resolution data set to 1.7 Å (native-2). For this, iterative cycles of refinement and model building with O were extended step-wise to 1.7 Å resolution. At 2 Å resolution water molecules were added to the model using the program ARP. After each refinement cycle, the model was checked against $2F_o$–F_c maps and manually adjusted to improve geometry and fit to the electron density. The model quality was checked with PROCHECK [69] which showed that 91% residues are within the most favored regions of the Ramachandran plot and only one residue, Ala124, exhibits a disallowed conformation.

Structure Solution of the Native and Complexed Trigonal Form

The trigonal structure was solved eventually at 2.1 Å resolution by molecular replacement with the monoclinic model. The trigonal and monoclinic models can be aligned with an rmsd value of 0.39 Å for 215 of the 321 Cα atoms.

The structure of the enzyme complexed with HA oligomer was obtained by cocrystallization of Hya (8 mg ml−1) in the presence of 4 mM of fluorescein-inated HA hexamer, using the hanging-drop method. The protein was mixed (1:1) with reservoir solution containing 25% PEG-4000, 0.2 M ammonium sulfate, 0.1 M Na-acetate (pH 4.6) and incubated over the reservoir. The complex structure was solved by molecular replacement with the final monoclinic model.

Acknowledgments

The technical assistance of Y. Rasser is greatly acknowledged. We thank George Orriss and Christine Wright for critical reading of the manuscript. We are grateful to the synchrotron staff at SRS in Daresbury, UK, and DESY, EMBL-outstation, Hamburg, Germany. This project was supported by Swiss National Foundation grant No. 31-50507 to Z. M.-H. and T. S.

Received: June 7, 2000
Revised: July 31, 2000
Accepted: August 3, 2000

References

1. Meyer, K. (1971). Hyaluronidases. In The Enzymes, 3rd Edition, Volume V, P.D. Boyer, ed. (New York: Academic Press), pp. 307–320.
2. Kreil, G. (1995). Hyaluronidases—a group of neglected enzymes. Protein Sci. *4*, 1666–1669.
3. Laurent, T.C. (1989). The Biology of Hyaluronan (New York: John Wiley & Sons).

4. Laurent, T.C., and Fraser, J.R.E. (1992). Hyaluronan. FASEB J. *6*, 2397–2404.
5. Lu, G., Kochoumian, L., and King, T.P. (1995). Sequence identity and antigenic cross-reactivity of white face hornet venom allergen, also a hyaluronidase, with other proteins. J. Biol. Chem. *270*, 4457–4465.
6. Gmachl, M., and Kreil, G. (1993). Bee venom hyaluronidase is homologous to a membrane protein of mammalian sperm. Proc. Natl. Acad. Sci. USA *90*, 3569–3573.
7. Frost, G.I., Csoka, T.B., Wong, T., and Stern, R. (1997). Purification, cloning, and expression of human plasma hyaluronidase. Biochem. Biophys. Res. Commun *236*, 10–15.
8. Lepperdinger, G., Strobl, B., and Kreil, G. (1998). Hyal2, a human gene expressed in many cells, encodes a lysosomal hyaluronidase with a novel type of specificity. J. Biol. Chem. *273*, 22466–22470.
9. Kemeny, D.M., Dalton, N., Lawrence, A.J., Pearce, F.L., and Vernon, C.A. (1984). The purification and characterisation of hyaluronidase from the venom of the honey bee, *Apis mellifera*. Eur. J. Biochem. *139*, 217–223.
10. Cramer, J.A., Bailey, L.C., Bailey, C.A., and Miller, R.T. (1994). Kinetic and mechanistic studies with bovine testicular hyaluronidase. Biochim. Biophys. Acta *1200*, 315–321.
11. Takagaki, K., et al., and Majima, M. (1994). Characterization of hydrolysis and transglycosylation by testicular hyaluronidase using ion-spray mass spectrometry. Biochemistry *33*, 6503–6507.
12. Primakoff, P., Lathrop, W., Woolman, L., Cowan, A., and Myles, D. (1988). Fully effective contraception in male and female guinea pigs immunized with the sperm protein PH-20. Nature *335*, 543–546.
13. Henrissat, B. (1991). A classification of glycosyl hydrolases based on amino acid sequence similarities. Biochem. J. *280*, 309–316.
14. Henrissat, B., and Bairoch, A. (1996). Updating the sequence-based classification of glycosyl hydrolases. Biochem. J. *316*, 695–696.
15. Soldatova, L., et al., and Mueller, U. (1998). Superior biological activity of the recombinant bee venom allergen hyaluronidase expressed in *Baculovirus*-infected insect cells as compared with *Escherichia coli.* J. Allergy Clin. Immunol *101*, 691–698.
16. Phillips, D.C. (1967). The hen egg-white lysozyme molecule. Proc. Natl. Acad. Sci. USA *57*, 484–495.
17. Perrakis, A., et al., and Vorgias, C.E. (1994). Crystal structure of bacterial chitinase at 2.3 Å resolution. Structure *2*, 1169–1180.
18. Divne, C., et al., and Jones, T.A. (1994). The three-dimensional crystal structure of the catalytic core of cellobiohydrolase I from *Trichoderma reesei*. Science *265*, 524–528.
19. Wakarchuk, W.W., Campbell, R.L., Sung, W.L., Davoodi, J., and Yaguchi, M. (1994). Mutational and crystallographic analyses of the active-site residues of the *Bacillus circulans* xylanase. Protein Sci. *3*, 467–475.
20. Mikami, B., Degano, M., Hehre, E.J., and Sacchettini, J.C. (1994). Crystal structures of soybean β -amylase reacted with β-maltose and maltal: active site components and their apparent roles in catalysis. Biochemistry *33*, 7779–7787.
21. Mikami, B., et al., and Utsumi, S. (1999). Structures of raw starch-digesting *Bacillus cereus* β-amylase complexed with maltose. Biochemistry *38*, 7050–7061.
22. Davies, G., and Henrissat, B. (1995). Structure and mechanism of glycosyl hydrolases. Structure *3*, 853–859.
23. Tews, I., Terwisscha van Scheltinga, A.C., Perrakis, A., Wilson, K.S., and Dijkstra, B.W. (1997). Substrate-assisted catalysis unifies two families of chitinolytic enzymes. J. Am. Chem. Soc *119*, 7954–7959.
24. Arming, S., Strobl, B., Wechselberger, C., and Kreil, G. (1997). *In vitro* mutagenesis of PH-20 hyaluronidase from human sperm. Eur. J. Biochem. *247*, 810–814.
25. Müller, U.R. (1990). Insect Sting Allergy (Stuttgart and New York: Gustav Fischer).
26. Müller, U.R., Crameri, R., and Soldatova, L. (1999). Diagnostik mit rekombinenten/synthetischen Bienengiftallergenen. Allergologie *22*, 51–52.
27. Banner, D.W., et al., and Waley, S.G. (1975). Structure of chicken muscle triose phosphate isomerase dermined crystallographically at 2.5 Å resolution using amino acid sequence data. Nature *255*, 609–614.
28. Henrissat, B., Callebaut, I., Fabrega, S., Lehn, P., Mornon, J.-P., and Davies, G. (1995). Conserved catalytic machinery and the prediction of a common fold for several families of glycosyl hydrolases. Proc. Natl. Acad. Sci. USA *92*, 7090–7094.
29. Eads, J.C., Ozturk, D., Wexler, T.B., Grubmeyer, C., and Sacchettini, J.C. (1997). A new function for a common fold: the crystal structure of quinolinic acid phosphoribosyltransferase. Structure *5*, 47–58.
30. Rouvinen, J., Bergfors, T., Teeri, T., Knowles, J.K.C., and Jones, T.A. (1990). Three-dimensional structure of cellobiohydrolase II from *Trichoderma reesei*. Science *249*, 380–386.
31. Spezio, M., Wilson, D.B., and Karplus, P.A. (1993). Crystal structure of the catalytic domain of a thermophilic endocellulase. Biochemistry *32*, 9906–9916.
32. Holm, L., and Sander, C. (1994). The FSSP database of structurally aligned protein fold families. Nucleic Acids Res. *22*, 3600–3609.
33. Davies, G.J., Wilson, K.S., and Henrissat, B. (1997). Nomenclature for sugar-binding subsites in glycosyl hydrolases. Biochem. J. *321*, 557–559.
34. Rao, V., Cui, T., Guan, C., and Van Roey, P. (1999). Mutations of endo-β-N-acetylglucosaminidase H active site residue Asp130 and Glu132: activities and conformations. Protein Sci.. *8*, 2338–2346.
35. Rao, V., Guan, C., and Van Roey, P. (1995). Crystal structure of endo-β-N-acetylglucosaminidase H at 1.9 Å resolution: active-site geometry and substrate recognition. Structure *3*, 449–457.
36. Terwisscha van Scheltinga, A.C., Hennig, M., and Dijkstra, B.W. (1996). The 1.8 Å resolution structure of hevamine, a plant chitinase/lysozyme, and analysis of the conserved sequence and structure motifs of glycosyl hydrolase family 18. J. Mol. Biol. *262*, 243–257.
37. Triggs-Raine, B., Salo, T.J., Zhang, H., Wicklow, B.A., and Natowicz, M.R. (1999). Mutations in HYAL1, a member of a tandemly distributed multigene family encoding disparate hyaluronidase activities, cause a newly described lysosomal disorder, mucopolysaccharidosis IX. Proc. Natl. Acad. Sci. USA *96*, 6296–6300.
38. McCarter, J.D., and Withers, S.G. (1994). Mechanisms of enzymatic glycoside hydrolysis. Curr. Opin. Struct. Biol *4*, 885–892.
39. Cleland, W.W., and Kreevoy, M.M. (1994). Low-barrier hydrogen bonds and enzymic catalysis. Science *264*, 1887–1890.
40. Zou, J.-Y., Flocco, M.M., and Mowbray, S.L. (1993). The 1.7 Å refined X-ray structure of the periplasmic glucose/galactose receptor from *Salmonella typhimurium.* J. Mol. Biol*. 233*, 739–752.
41. Zou, J.-Y., et al., and Jones, T.A. (1999). Crystallographic evidence for substrate ring distortion and protein conformational changes during catalysis in cellobiohydrolase Cel6A from *Trichoderma reesei.* Structure *7*, 1035–1045.
42. Van Roey, P., Rao, V., Plummer, T.H., Jr., and Tarentino, A.L. (1994). Crystal structure of endo-β-N-acetylglucosaminidase F_1, an α/β-barrel enzyme adapted for a complex substrate. Biochemistry *33*, 13989–13996.
43. Matsumoto, T., Nonaka, T., Hashimoto, M., Watanabe, T., and Mitsui, Y. (1999). Three-dimensional structure of the catalytic domain of chitinase A1 from *Bacillus circulans* WL-12 at a very high resolution. In Proceedings of the Japan Acadamy Series B-Physical and Biological Sciences *75*, 269–274.
44. Flocco, M.M., and Mowbray, S.L. (1995). Strange bedfellows: interactions between acidic sidechains in proteins. J. Mol. Biol. *254*, 96–105.
45. Tews, I., Perrakis, A., Oppenheim, A., Dauter, Z., Wilson, K.S., and Vorgias, C.E. (1996). Bacterial chitobiase structure provides insight into catalytic mechanism and the basis of Tay-Sachs disease. Nat. Struct. Biol. *3*, 638–648.
46. Davies, G.J., Withers, S.G., et al. (1998). Snapshots along an enzymatic reaction coordinate: analysis of a retaining β-glycoside hydrolase. Biochemistry *37*, 11707–11713.
47. Ford, L.O., Johnson, L.N., Machin, P.A., Phillips, D.C., and Tjian, R. (1974). Crystal structure of a lysozyme-tetrasaccharide lactone complex. J. Mol. Biol. *88*, 349–371.
48. Strynadka, N.C.J., and James, M.N.G. (1991). Lysozyme revisited: crystallographic evidence for distortion of an N-acetylmuramic acid residue bound in site D. J. Mol. Biol. *220*, 401–424.
49. Hadfield, A.T., et al., and Johnson, L.N. (1994). Crystal structure of the mutant D52S hen egg white lysozyme with an oligosaccharide product. J. Mol. Biol. *243*, 856–872.
50. Kuroki, R., Weaver, L.H., and Matthews, B. (1993). A covalent enzyme–substrate intermediate with saccharide distortion in a mutant T4 lysozyme. Science *262*, 2030–2034.
51. Sulzenbacher, G., Driguez, H., Henrissat, B., Schulein, M., and Davies, G. (1996). Structure of the fusarium oxysporum endoglucanase I with a nonhydrolyzable substrate analogue: substrate distortion gives rise to the preferred axial orientation for the leaving group. Biochemistry *35*, 15280–15287.
52. Rouvinen, J., et al., and Mantyjarvi, R. (1999). Probing the molecular basis of allergy. Three-dimensional structure of the bovine lipocalin allergen Bos d 2. J. Biol. Chem. *274*, 2337–2343.

53. Lascombe, M.-B., et al., and Alzari, P.M. (2000). Crystal structure of the allergen Equ c 1. J. Biol. Chem. *275*, 21572–21577.
54. De Marino, S., et al., and Pastore, A. (1999). An immunoglobulin-like fold in a major plant allergen: the solution structure of Phl p 2 from timothy grass pollen. Structure *7*, 943–952.
55. Thorn, K.S., et al., and Schutt, C.E. (1997). The crystal structure of a major allergen from plants. Structure *5*, 19–32.
56. Fedorov, A.A., Ball, T., Mahoney, N.M., Valenta, R., and Almo, S.C. (1997). The molecular basis for allergen cross-reactivity: crystal structure and IgE-epitope mapping of birch pollen profilin. Structure *5*, 33–45.
57. Ichikawa, S., et al., and Inagaki, F. (1998). Solution structure of Der f *2*, the major mite allergen for atopic diseases. J. Biol. Chem. *273*, 356–360.
58. Miller, S., Janin, J., Lesk, A.M., and Chothia, C. (1987). Interior and surface of monomeric proteins. J. Mol. Biol. *196*, 641–656.
59. Laver, W.G., Air, G.M., Webster, R.G., and Smith-Gill, S.J. (1990). Epitopes on protein antigens: misconceptions and realities. Cell *61*, 553–556.
60. Ferreira, F., et al., and Scheiner, O. (1998). Modulation of IgE reactivity of allergens by site-directed mutagenesis: potential use of hypoallergenic variants for immunotherapy. FASEB J. *12*, 231–242.
61. West, D.C., and Shaw, D.M. (1998). Tumour hyaluronan in relationship to angiogenesis and metastasis. In The Chemistry and Biology and Medical Applications of Hyaluronan and Its Derivatives, T.C. Laurent and E.A. Balazs, eds. (Colchester, UK: Portland Press, Wenner-Gren International Series No.72), pp. 227–233.
62. Leslie, A.G.W. (1992). Joint CCP4 and ESF-EACBM Newsletter on Protein Crystallography No. 26. SERC Daresbury Laboratory, Warrington, UK.
63. Collaborative Computational Project Number 4. (1994). The CCP4 suite: proteins for crystallography. Acta Crystallogr. D *50*, 760–763.
64. de La Fortelle, E., and Bricogne, G. (1997). Maximum-likelihood heavy-atom parameter refinement for multiple isomorphous replacement and multiwavelength anomalous diffraction methods. Methods Enzymol. *276*, 472–494.
65. Abrahams, J.P., and Leslie, A.G.W. (1996). Methods used in the structure determination of bovine mitochondrial F_1 ATPase. Acta Crystallogr. D *52*, 30–42.
66. Jones, T.A., Zou, J., Cowan, S., and Kjeldgaard, M. (1991). Improved methods for binding protein models in electron density maps and the location of errors in these models. Acta Crystallogr. A *47*, 110–119.
67. Cowtan, K.D., and Main, P. (1996). Phase combination and cross validation in iterated density-modification calculations. Acta Crystallogr. D *52*, 43–48.
68. Navaza, J. (1994). Amore: an automated package for molecular replacement. Acta Crystallogr. A *50*, 157–163.
69. Laskowski, R.A., MacArthur, M.W., Moss, D.S., and Thornton, J.M. (1993). Procheck: a program to check the stereochemical quality of protein structures. J. Appl. Crystallogr *26*, 283–291.
70. Jacobson, R.S., Hoffman, D.R., and Kemeny, D.M. (1992). The cross-reactivity between bee and vespid hyaluronidases has a structural basis. J. Allergy Clin. Immunol *89*, 292.
71. Read, R.J. (1986). SIGMAA-Improved Fourier coefficients for maps using phases from partial structures with errors. Acta Crystallogr. A *42*, 140–149.
72. Brünger, A.T., et al., and Warren, G. (1998). Crystallography and NMR system: a new software suite for macromolecular structure determination. Acta Crystallogr. D *54*, 905–921.
73. Jain, S., Drendel, W.B., Chen, Z., Mathews, F.S., Sly, W.S., and Grubb, J.H. (1996). Structure of human β-glucuronidase reveals candidate lysosomal targeting and active-site motifs. Nat. Struct. Biol. *3*, 375–381.
74. Burmeister, W.P., Cottaz, S., Driguez, H., Iori, R., Palmieri, S., and Henrissat, B. (1997). The crystal structures of *Sinapis alba* myrosinase and a covalent glycosyl-enzyme intermediate provide insights into the substrate recognition and active-site machinery of an *S*-glycosidase. Structure *5*, 663–675.
75. Leggio, L.L., Kalogiannis, S., Bhat, M.K., and Pickersgill, R.W. (1999). High resolution structure and sequence of *T. aurantiacus* xylanase I: implications for the evolution of thermostability in family 10 xylanases and enzymes with (β)α-barrel architecture. Proteins *36*, 295–306.

Protein Data Bank Accession Codes

Coordinates and structure factors have been deposited in the Protein Data Bank with accession codes 1FCQ (native monoclinic data), 1FCU (native trigonal data) and 1FCV (trigonal form in complex with the HA tetramer).